applied optics

Integrated multimode optical waveguides in glass using laser induced deep etching

Birger Reitz,[1,2,*] Andreas Evertz,[1] Robin Basten,[2,3] Marc Christopher Wurz,[2,3] and Ludger Overmeyer[1,2]

[1]Leibniz University Hannover, Institute of Transport and Automation Technology, Garbsen, Germany
[2]Cluster of Excellence PhoenixD (Photonics, Optics and Engineering–Innovation Across Disciplines), Hannover, Germany
[3]Leibniz Universität Hannover, Institute of Micro Production Technology, Garbsen, Germany
*birger.reitz@ita.uni-hannover.de

Glass is an ideal material for optical applications, even though only a few micromachining technologies for material ablation are available. These microstructuring methods are limited regarding precision and freedom of design. A micromachining process for glass is laser induced deep etching (LIDE). Without generating micro-cracks, introducing stress, or other damages, it can precisely machine many types of glass. This work uses LIDE to subtractive manufacture structures in glass carrier substrates. Due to its transmission characteristics and refractive index, the glass substrate serves as optical cladding for polymer waveguides. In this paper, the described fabrication process can be divided into two sub-steps. The doctor blade technique and subsequent additive process step is used in manufacturing cavities with U-shaped cross-sections in glass in order to fill the trenches with liquid optical polymers, which are globally UV-cured. Based on the higher refractive index of the polymer, it enables optical waveguiding in the visible to near-infrared wavelength range. This novel, to the best of our knoowledge, manufacturing method is called LDB (LIDE-doctor-blade); it can be the missing link between long-distance transmissions and on-chip solutions on the packaging level. For validation, optical waveguides are examined regarding their geometrical dimensions, surface roughness, and waveguiding ability, such as intensity distribution and length-dependent attenuation.

https://doi.org/10.1364/AO.506670

1. INTRODUCTION

Increasing data volumes in industrial and private sectors require reliable and fast transmission solutions. Unlike optical communication, traditional signal transmission using copper cables is susceptible to electromagnetic interference. In addition, a much larger amount of data can be transmitted with light than conventional methods, either over long distances, even between continents using fibers, or via short on-chip solutions. On-chip devices are usually produced using silicon-based lithographic manufacturing processes called photonic integrated circuits (PIC). However, it is expensive due to costly mask manufacturing and complex production processes, and even minor changes are associated with high effort. In addition, many production facilities for the required processes are severely limited in their work space and thus do not allow large-scale production.

Glass has excellent advantages for many applications, as it can be used industrially in high volumes and is flexible in its utilization. In particular, optical transparency, electrical insulation, mechanical strength, and the adjustable coefficient of thermal expansion play a significant role. Controlled encapsulation of optically active materials allows the fabrication of advanced functional glasses, making it a very interesting and versatile material for optoelectronic applications [1,2]. Furthermore, glass is cheaper than silicon and can be produced and processed in large formats.

Chen *et al.* and Tunon *et al.* have outlined a technique to increase the refractive index through femtosecond laser modification locally. This innovative approach enables the direct utilization of the written path as the core of an optical waveguide [3–6]. Typically, amorphous glass serves as a carrier substrate, as well as cladding material, in this process. Achieving structural resolutions on the order of single-digit micrometers allow the production of circular single-mode-capable optical waveguides [7]. This method provides significant versatility, facilitating the creation of three-dimensional networks within a substrate. Optical attenuations of waveguides range from 0.062 up to 5.3 dB/cm [4,5,6]. However, achieving these results necessitates highly precise axis systems in three spatial directions and extensive parameter investigations concerning pulse energy,

repetition rate, and writing speed, as these parameters substantially influence the cross-sectional shape of the waveguide. Righini and Chiappini have reported that such structures may not exhibit long-term durability and can be vulnerable to environmental effects [8].

An alternative approach to fabricating integrated optical waveguides in glass involves ion exchange at the substrate surface [9]. Schröder *et al.* have already fabricated integrated optical waveguides in glass as a coupling element. In lithographic manufacturing, an ion-exchange process is used in which silver ions replace sodium ions and thus provide an increase in the refractive index. This enables total reflection waveguiding in glass. This manufacturing process entails several photolithographic steps to establish a near-surface optical waveguide core buried within the substrate, employing two successive ion exchange processes. Thin glass substrates can be processed, measuring up to 440 mm × 350 mm with a thickness ranging from 300 to 550 µm, achieving a patterning resolution of less than 20 µm [10]. However, it's important to note that due to a low refractive index difference, as indicated by Brunsberg *et al.*, curvatures with a radius of less than 30 mm result in significant optical losses with this method and processes employing laser direct writing [3,11]. Nevertheless, achieving masked production requires more substantial effort and high costs [12].

In addition, a method for micromachining glass can also close the gap between extremely short and long transmission distances. Near-surface optical waveguides can be manufactured by targeted material removal and subsequent filling with optical core material. Our manufacturing method is called LDB (LIDE-doctor-blade); it combines the subtractive material ablation with the LIDE process and the filling technique with liquid polymer by using doctor blading. Complex shapes and geometries can be produced cost effectively, which can variably

function as an interconnect on the PCB level to be part of the package between extremely short and long transmission paths. This allows the component to be considered an electro-optical printed circuit board (EOCB). This is a circuit board that integrates electronic and optical components to enable signal processing and transmission within a single device. This concept combines the advantages of electronic signal processing with optical data transmission [10,13–16]. Due to the flexibly designable geometries, optical splitters, combiners, or other structures can be manufactured to form an optical network. Figure 1 shows possible visionary application scenarios for the glass platform. Individual fibers can be coupled to the platform via V-grooves or directly in a fiber array. Additionally, the manufacturing process can produce pockets to align discrete components passively. Furthermore, conductor trays or vertical interconnects access (VIA) for electrical connections can be realized directly on the substrate. Thus, by suitable arrangement of the integrated optical waveguides, evanescent couplers [17], Mach–Zender interferometers [18,19], ring resonators [20,21], or similar functional elements can be implemented. However, a single-mode data transmission is required to realize most of these elements, which can be achieved through continuous process improvement in the future. A PIC is shown in the center of the glass, connected optically via photonic wire bonds or direct coupling and electrically via conventional wire bonds. Though different applications can be covered with this technique, the connection to micro-electro-mechanical systems (MEMS) or to the field of fiber optics is possible as well. The optical fiber broadband network structure for providing all or part of the local loop used for the last mile of telecommunications is called fiber-to-the X (FTTX). This requires a complex, bulky setup to split the signal. This element can be substituted with an integrated EOCB. These visionary concepts are the
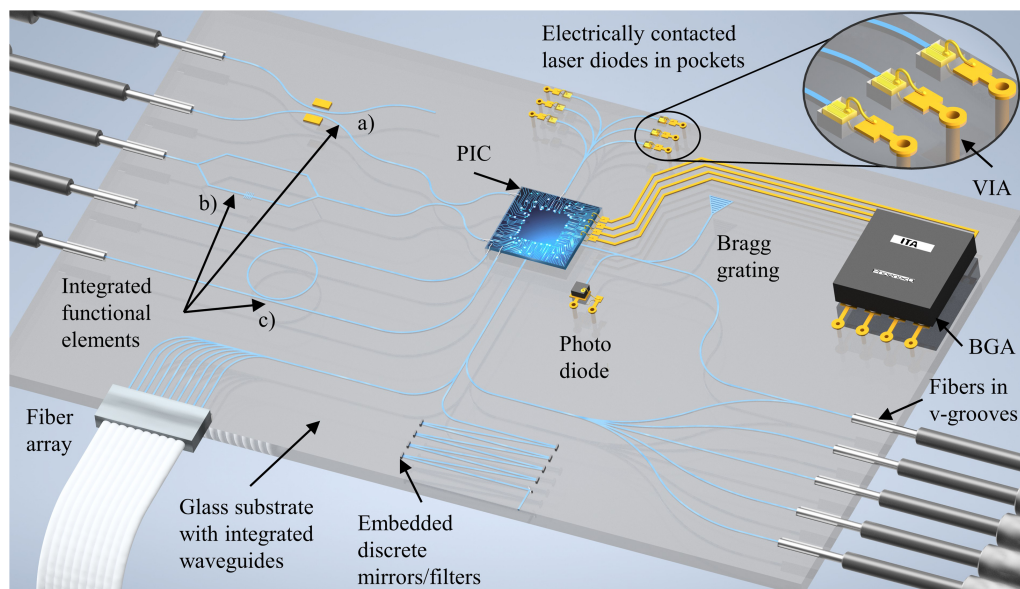
Fig. 1.   Possible visionary application scenarios for the glass platform, which combines discrete electrical components such as ball grid arrays (BGA) or laser diodes, as well as passive and active optical structures. It represents an interface technology between long transmission options in the form of optical fibers and compact photonic integrated circuits (PIC). An external coupling for optical fibers in U-shaped cavities is shown, which connects the central PIC through network structures in the glass. Furthermore, possible future structural elements, such as (a) evanescent couplers [17], (b) interferometers [18,19], and (c) ring resonators [20,21] can be seen.
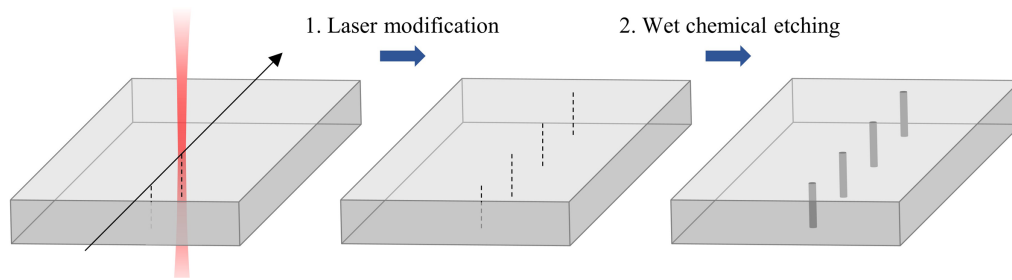
Fig. 2. LIDE process steps for manufacturing microstructures in glass substrates.

primary goal of this field of research. However, it must first be characterized in detail to ensure that the manufacturing process for integrated LDB optical waveguides in glass trenches is feasible.

2. PROCEDURE

This section presents a process for microstructuring thin glass surfaces to implement cavities. These microstructures are filled with a transparent photopolymer that serves as a core material for waveguiding due to the suitable refractive indices. The glass carrier substrate also functions as an optical cladding for the embedded integrated optical waveguide. Our process chain, combining a subtractive followed by an additive manufacturing process to manufacture optical waveguides, is called the LDB method.

A. Microstructuring of Glass

Traditionally, structures in glass are either ablated directly, using a laser, or removed by mask-based etching. However, these methods have some disadvantages regarding surface roughness, aspect ratio, and process-induced shape defects such as undercuts [22,23]. A combination of laser modification and subsequent global etching is a gentler glass process. Selective laser-induced etching (SLE) is a two-step process for creating three-dimensional structures in or on various types of glass. Ultrashort pulsed laser radiation is focused into the transparent volume of the workpiece in the first step. In a multiphoton process, the pulse energy is only absorbed in the focused volume. As a result, the material is modified without cracking, thus changing its chemical properties. This allows the structured section to be chemically etched selectively later. Connected areas can be modified by shifting the focus in the workpiece using a microscanner system. Solid structures can then be removed by wet chemical etching in a second process step. Microchannels, molded holes, structural elements, and complex mechanical composites can be produced. Root-mean-square roughness (R_q) values in the modified areas from about 1 μm to as low as 200 nm are achievable [24–26].
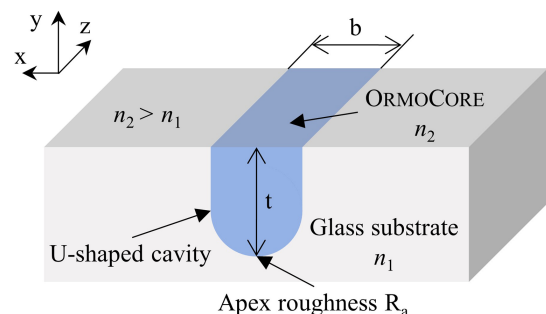
Another much faster process for high-precision micromachining of thin glass is the laser-induced deep etching (LIDE) process from LPKF Laser & Electronics AG. It is protected by patents [27,28], and the laser parameters are confidential. It has been developed for high-precision micromachining of thin glass. This technology also aims to manufacture through holes, micro-cuts, or cavities. In contrast to the SLE process, which

requires a focused spot with energy densities below the ablation threshold, individual defocused laser pulses are used to modify the glass across its entire thickness, as shown in Fig. 2. During maskless wet etching, the glass is removed, which occurs isotropically across its whole surface, leading to a thickness reduction. At the same time, laser-modified regions etch at much higher rates. This avoids mechanical and thermal stress in glass that occurs with direct laser ablation [29–31]. Silicate-based glass types can be processed, with substrate thicknesses ranging from 50 μm up to 1000 μm. LPKF's laser modification systems can process substrates up to 510 mm in edge length [32].
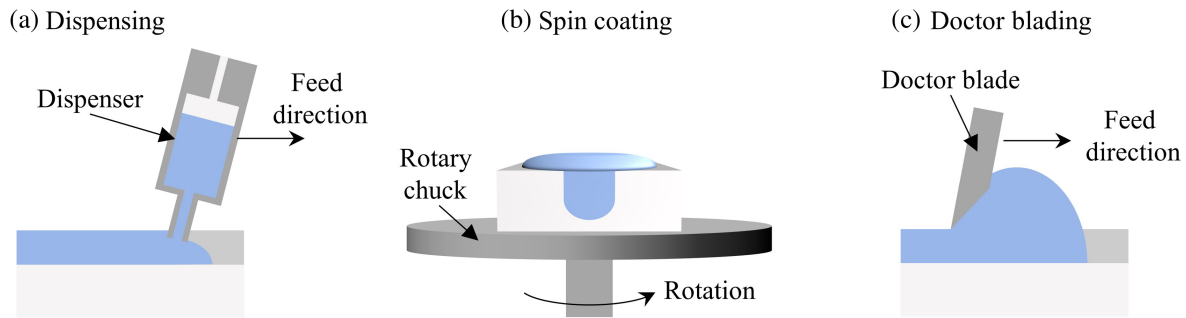
With this process, structure sizes smaller than 5 μm can be achieved. A significant advantage over other approaches is the achievable high aspect ratio of 10:1 or even 50:1 under certain conditions. Compared to that in traditional masked wet chemical etching, only aspect ratios smaller than 1:1 can be achieved due to the amorphous crystal structure of glass. Glass structured by LIDE exhibits the same mechanical strength as the starting material since defects such as micro cracks or chipping are not generated in the first place. Furthermore, LIDE offers a high throughput of several thousand holes per second, as only a single laser pulse is required for individual microstructures. Typically, the process is used to fabricate interposers or other components in optical and electronic packages [33]. Near-surface microstructures are manufactured into glass for waveguide production by modifying a 2D path on its surface with single laser pulses. Due to the glass's material properties, the grooves have a U-shaped cross section [34].

B. Optical Waveguide Manufacturing

Figure 3 shows a principal sketch of an integrated optical waveguide in a U-shaped cavity. Various fluids, which can be cured, are considered for cavity filling. Due to the low shrinkage after curing, its high viscosity, and thus good handling, OrmoCore

Fig. 3. Integrated waveguide structure in a U-shaped glass cavity.

(a) Dispensing

Dispenser

Feed direction

(b) Spin coating

Rotary chuck

Rotation

(c) Doctor blading

Doctor blade

Feed direction

Fig. 4. Three manufacturing methods for filling glass cavities with liquid material to fabricate integrated optical waveguides: dispensing [35,36], spin coating [37], and doctor blading [38].

by micro resist technology is chosen. It also has good optical properties, such as a higher refractive index than glass and high transmission characteristics. Its refractive index in the solid state is $n_2 = 1.555$, while the two examined glasses have the following indices: $n_{1,\text{MemPax}} = 1.47$ and $n_{1,\text{AF32}} = 1.51$.

For filling the cavities with core polymer, manufacturing processes, such as spin coating, doctor blading, and direct application with the help of a microdispenser, are considered. These three manufacturing variants are outlined in Fig. 4. In a dispensing process, fluid material is squeezed through a nozzle and applied locally onto or into a substrate. To do so, either the substrate or the dispenser is directly actuated. Process parameters are translation speed and volume flow rate, which can be adjusted by the dispensing pressure depending on the fluid. In addition, a few process characteristics also rely on the dispenser needle. When filling structures in the range of several hundred micrometers, high accuracies are required for the axis' movement and the nozzle quality [35,36,39]. With optimally selected parameters, the substrate has little fluid residue because only as much fluid as necessary is applied. The demands on path planning increase with the complexity of the design of the cavities. This manufacturing technique can realize simple geometries, such as straight or slightly curved paths. Branched complex network structures are complicated to produce with this process. Furthermore, the processing speed is low because each path has to be processed sequentially [40]. As a result of the high accuracy and associated effort, this process is unsuitable for the application described.

The polymer application using spin coating is independent of the optical waveguide path. In this process, the carrier substrate is mounted on a rotating chuck with fluid applied to the sample. A resulting coating film is influenced by acceleration, rotational speed, and the process duration [37,41]. Spin coating is widely represented in lithographic processes with mask-based curing, where layer thicknesses of less than 5 μm are required [42–45]. By spreading the fluid entirely over the substrate, sufficient quality to guarantee cavity flooding is ensured.

Like spin-coating processes, the microstructure's complexity does not influence polymer application using doctor blading. A surplus amount of fluid is moved over the substrate by a metallic doctor blade with a chamfer on its contact edge. This process can be used to fill any planar structure. Depending on the contact pressure and feed rate, no fluid residue remains as the excess material is completely wiped off the sample. A

chamfer or tilting of the entire doctor blade is necessary, as this enormously reduces the occurrence of the stick-slip effect [46]. Structures with a resolution of down to 10 μm can be filled using this method; for smaller structure sizes, the high fluid viscosity $(2.9 \pm 0.4 \, \text{Pa} \cdot \text{s})$ does not ensure a filled groove [47,48]. In this work, for filling the integrated cavities in the x-direction, the COATMASTER 510 from ERICHSEN is used for the semi-automated doctor-blading process of the planar samples. Regardless of the manufacturing strategy used to fill the cavities, it is necessary to cure the fluid globally. For exposure, the materials are cured in the wavelength range from 300 to 400 nm with a power of $6 \, \text{W/cm}^2$ for 2 s. Since a slightly longer exposure time has no adverse effect on the fluid, the duration specified by the polymer supplier is exceeded to guarantee complete curing.

For measuring the optical properties of the waveguides, it is necessary to prepare end facets of the cavities to couple light in. Generally, grooves up to the edge of the glass substrate are technically possible. However, the grooves would have an uneven cross section since, during the etching process, the pre-structured paths are ablated additionally from the side. Therefore, grooves would reach deeper at these locations, which results in liquid flow out from the edges. Thus, the degree of filling at the end facets would be significantly reduced. Critical edge pieces are removed from the substrate to ensure that the cavities are filled evenly along their length. Similar to glass fiber cleaving, controlled removal creates a surface with optical quality. Therefore, a predetermined breaking line is created on the substrate backside using a thin glass cutting tool. This glass cutter uses a rotating diamond blade, which provides approximately 10 μm rectangular cavities in the glass at a 1.5 μm depth and a 5 μm width. At this predetermined breaking line, the glass is fixated on a support with a sharp edge for optimum breakage, and the overhanging glass is bent in the backside direction.

3. RESULTS

In this chapter, unfilled microstructures and filled cavities are investigated geometrically and then characterized optically in terms of intensity distribution and their attenuation based on their geometry.

A. Geometrical Characterization

The choice for the geometric target size of the structured paths in the glass is based on commercial multimodal glass
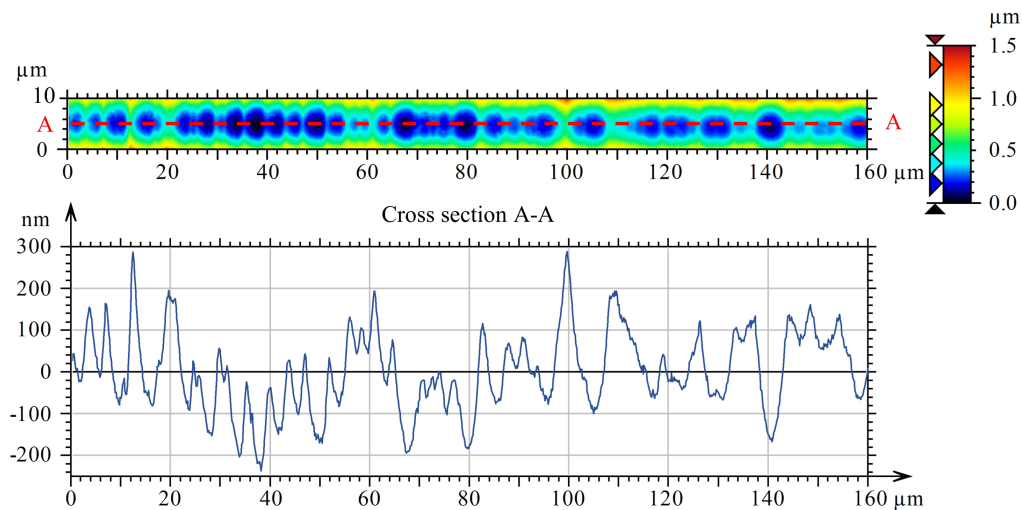
Fig. 5. Topography measurement of the apex' contour, below Cross section (A-A) along the measured area, glass type: MemPAX.

fibers with a core diameter of 50 μm. Therefore, a width of the U-shaped structures of 50 μm is targeted. The cavities' depth results from etching time and glass type. In principle, all commercially available silicate-based glass types can be processed with the LIDE method. For this, two types are compared. The MemPAX is a borosilicate glass with a density of 2.22 g/cm³, an electric volume resistivity of $1.18 \cdot 10^8$ Ω·cm (at 250°C) and a spectral transmittance of 92,8 % in the visible to near-infrared wave range. AF 32 ECO is an alkali-free borosilicate glass with a density of 2.43 g/cm³, an electric volume resistivity of $7.9 \cdot 10^{11}$ Ω·cm (at 250°C) and a spectral transmittance of 92,1 % in the same wavelength range. The two types of glass from SCHOTT have similar material properties but show differences when processed with LIDE. The manufactured structures have a mean width at the surface of $b_{MemPAX} = 49.873 \pm 0.329$ μm ($n = 72$). The average depth of the cavities is $t_{MemPAX} = 43.429 \pm 4.190$ μm. Surface roughness has a strong influence on the optical compatibility of the system. The higher the roughness, the higher the optical loss since light is reflected unevenly and uncontrollably at the interfaces [49,50]. Figure 5 below shows surface roughness distribution R_a at the U-shaped cavity's apex. The center roughness R_a for the MEMpax glass is $R_{a,MemPAX} = 58.642 \pm 11.897$ nm, with both visible and near-infrared light, $R_a < \lambda/10$.

Compared to the MemPAX glass, the AF 32 ECO glass shows similar values in width, $b_{AF32} = 49.95 \pm 0.518$ μm. The groove's depth shows a difference between both glass types; structures in the AF 32 ECO glass have a mean depth of $t_{AF32} = 50.754$ μm with a standard deviation of $\sigma = 4.702$ μm ($n = 36$). Higher depth values indicate a higher etch rate of the pre-patterned surfaces of the AF 32 ECO glass than those of the MemPAX glass since process steps to obtain the microstructures are the same. These material properties are nearly insignificant for subsequent optical use, but the surface roughness values of the contour are not. AF 32 ECO has significantly higher roughness values, $R_{a,AF32} = 456.015 \pm 384.469$ nm. A topographic measurement of the contour at the apex is visualized in Fig. 5. The cross section shows the individual laser pulses, each creating

a half ellipsoid in the glass after the etching process. Such an overlap of the pulses creates a continuous trench. The surface roughness causes scattering of the transmitted light when it hits the interface. Since the cavities of the MemPAX glass have significantly lower roughness values, this glass is used for filling from now on.

Figure 6 shows two frontal views of filled U-shaped cavities. On the left, the cavity has been filled by spin coating, while the right-hand view shows the front face of a doctor-bladed optical waveguide. With both processes, the cavities are filled, but with spin coating, an additional layer forms over the surface. The samples are coated for 40 s at a maximum speed of 5000 RPM. Even at maximum speed, a layer forms with an average height of 15.37 ± 2.72 μm ($n = 15$). Increasing the rotational speed reduces the height of the film, but it cannot be avoided entirely and causes massive optical losses when light is coupled into the waveguide. Light is scattered uncontrollably over the entire surface; only minimal amounts are transmitted in the waveguide. For this reason, spin coating without post-processing is also unsuitable for this application; in addition, this process can cause the cured polymer to come loose from the trench.

In the following section, surface roughness of the end facets is analyzed. Therefore, only end facets are accounted for, which have not entailed any obvious defects from the breaking process. The arithmetic mean surface roughness value is $S_{a,u} = 102.876$ nm, with a standard deviation of 57.98 nm ($n = 34$). For comparison, mechanically cleaved glass fibers have a mean surface roughness of $S_{a,fiber} = 48.44 \pm 24.96$ nm ($n = 31$). However, it cannot be clearly stated whether this is exclusively due to breaking since small crack-like structures can also be caused due to the curing process. Furthermore, the shrinkage due to curing can be seen, especially on the right side of the figure. The transformation from the liquid to the solid state reduces the volume by 2 %–5 %.

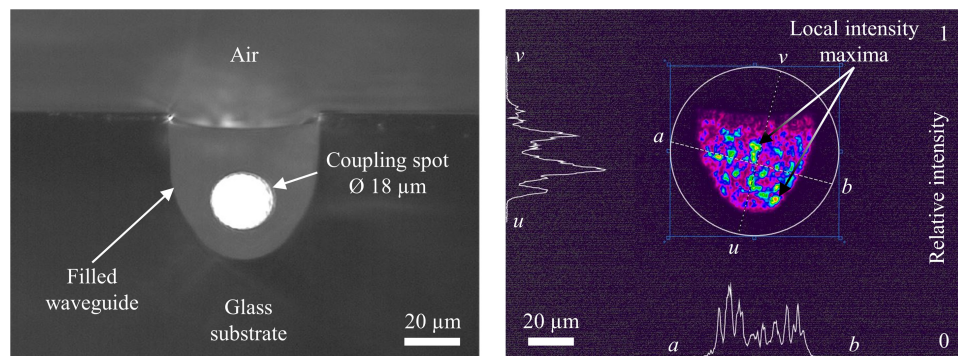## B. Intensity Distribution and Optical Properties

For measuring the optical attenuation, light that is coupled into the waveguide is detected at the output end to determine both
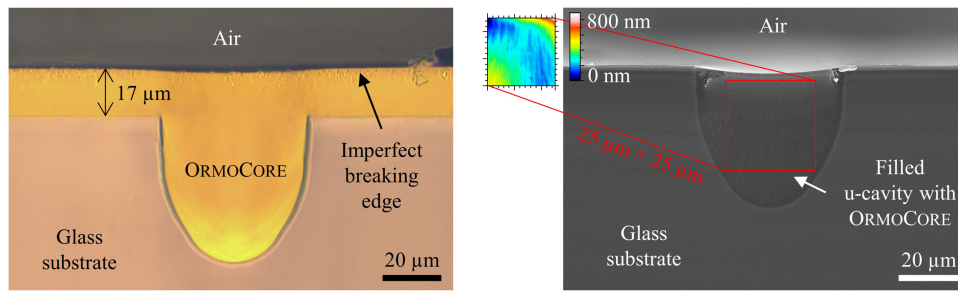
Fig. 6. End facet views of filled U-shaped cavities. Spin coating (microscope image, left). Doctor blading (SEM image, right).
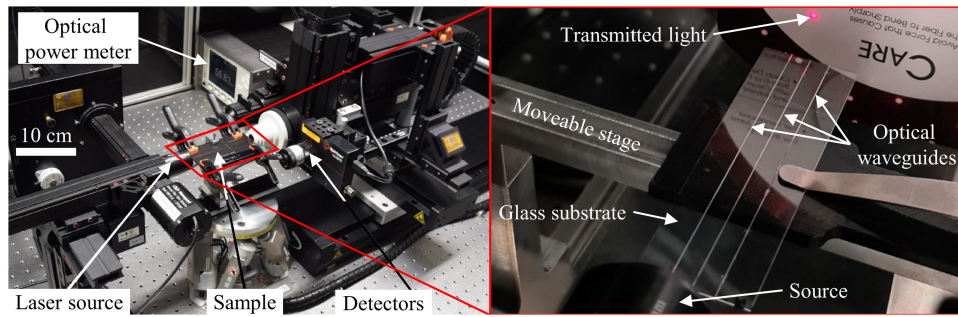
Fig. 7. Optical measurement setup for waveguide characterization.

Fig. 8. Camera view of coupling with a spot diameter of 18 μm into a U-shaped light waveguide (left). Relative intensity distribution of a doctor-bladed optical waveguide in a U-shaped cavity (right).

intrinsic and extrinsic losses of the transmission path. For this purpose, a laser with a central wavelength of 638 nm is used for this specially developed measurement setup [50,51]. The measuring setup can be seen in Fig. 7; the sample is fixed on a moveable stage to ensure optimal coupling efficiency. The projected spot has a diameter of 18 μm; this procedure is shown in Fig. 8 on the left. Light is coupled into the waveguide with a small numerical aperture of NA = 0.1 and an average optical power of $P_{in} = 613 \pm 113$ nW. The transmitted power P_{out} is measured with a collecting lens on a photodetector.

By calculating the logarithmic ratio between the input power P_{in} and the output power P_{out}, the total attenuation a in dB of the waveguide can be determined as follows:

$$A = 10 \cdot \log_{10}\left(\frac{P_{in}}{P_{out}}\right). \tag{1}$$

Since each optical waveguide varies from another, the losses are distributed unevenly. Therefore, the total attenuation

specification is unsuitable for a sufficient analysis. As mentioned, quality of the carrier material, the production technique, and the surface quality of the optical waveguides significantly influence low-loss transmission. In addition, extrinsic influences also have a negative effect on this. The so-called cut-back method distinguishes between attenuation in the waveguide and coupling losses [52,53]. With this method, optical attenuation of a sample is determined, and afterward, the sample is shortened and measured again. By a successive length reduction of the transmission path, length-dependent attenuation can be defined as follows:

$$\frac{a}{l} = \frac{a_1 - a_2}{l_1 - l_2}. \tag{2}$$

The value l_i indicates the length in cm, and a_i indicates the optical attenuation in dB of sample i. So, the constant part, independent of the specimen's length, is due to the coupling site, the front surface quality, or the measuring site [52].

1. Length-Dependent Attenuation of Linear Optical Waveguides

First, optical waveguides without junctions or bends are examined. To characterize the integrated U-shaped optical waveguides, 15 samples from the same production batch are measured three times each to minimize stochastic error influences. A sample length of 65 mm is targeted. Since the marking and subsequent breaking are performed manually, it can lead to minor length changes between each other. In Fig. 8, the intensity distribution of such a waveguide on the output is shown on the right side; local maxima are formed, and the power is evenly distributed, which is typical for a multimode optical waveguide. However, it should be noted that the local intensity decreases slightly towards the upper break edge, which can also be seen in the vertical intensity profile on the left ($u - v$). This may be caused by the resulting compressive force during breakage.

Determined attenuation values range from 7.49 dB to 16.8 dB. From the experiments, an average optical attenuation of $a_u = 11.61$ dB with a standard deviation of 2.57 dB is obtained. To distinguish between the intrinsic attenuation in the optical waveguide and the extrinsic coupling losses, five glass substrates are shortened four times by about 2 mm each. It is ensured that only one side is cut back, and the outcoupling side remains unchanged. Each breaking process modifies the surface quality of the waveguide's end facet, so the optical attenuation might appear higher for a shorter sample than for the longer one since the end facet's quality has worsened. Using formula (2), a negative length-dependent attenuation results, which would correspond to an energy increase through the optical waveguide, which is not possible through the given experimental setup. Therefore, such measured values (quantity < 10 %) are not considered further. Average length-dependent attenuation is $a_u/l = 0.258 \pm 0.204$ dB/cm. Material-specific values of approximately 0.1 dB/cm ($\lambda = 633$ nm) is possible with optimal use, according to the manufacturer of OrmoCore. With an original specimen length of 65 mm, the intrinsic loss corresponds to 1.677 ± 1.326 dB. This means the facets cause most attenuation losses at 9.93 ± 1.244 dB. Such coupling losses can occur from back reflections or formation of stray light due to an inhomogeneous surface because of the breaking process. Compared to other waveguides without using complex lithography process steps, the length-dependent attenuation of LDB waveguides show reasonable characteristics, as shown in Table 1.

2. Curved Waveguides

In integrated waveguide network structures, different shapes and geometries are combined. The properties of linear structures have already been presented geometrically and optically, so the influence of the radius of curvature of the cavity is investigated next. Therefore, a design for characterization is created, which allows an investigation of different radii of curvature. The influence of radii in the 10–50 mm range is considered. A path consists of two straight sections (s_g), two curved sections (s_r), and, if necessary, an oblique section (s_l). The substrate has a width of 90 mm. Starting from the 5th path with a radius of curvature of 50 mm, the arc length is determined since this path does not require an oblique intermediate section to ensure a uniform and comparable length among all paths. The specimen design for the different radii of curvature is shown in Fig. 9.

From previous measurement results, the length-dependent attenuation in the curved sections of the geometries is determined approximately. The average attenuation of $a/l = 0.26$ dB/cm for the straight-line segments is assumed. The resulting value of the straight-line segments is subtracted from the determined attenuation values. Furthermore, a coupling attenuation of 9.92 dB is also considered. The remaining values in the curve segments are related to the respective arc lengths of the curves, resulting in the right-hand diagram of Fig. 9. It shows the individual attenuation as a function of the radius of curvature. Four different samples are shown; it is noticeable that the curves of samples $1 + 2$ and $3 + 4$ are very similar. However, the characteristic of sample pair $3 + 4$ is higher, which indicates unclean end facets or contamination in the waveguide. Nevertheless, qualitative behavior is evident between all four samples; with a larger radius of curvature, the attenuation decreases tremendously. Since the angle of incidence at the interfaces increases with smaller radii, more power is coupled out of the waveguide and is no longer transmitted [11,54,60–63]. The difference from the smallest radius of 10 mm to the radius of 20 mm results in an average reduction in attenuation of 52 %, regardless of which specimen is used. For an infinitely large radius, so no curvature, the value tends toward the length-dependent attenuation $a/l = 0.258 \pm 0.204$ dB/cm of straight sections.

Compared to Wolfer's printed optical waveguides with a similar scale, the waveguides in the U-shaped cavities have significantly lower attenuation values ($a_{15\,mm\_wolfer} = 8.35$ dB/cm versus $a_{10\,mm-reitz} = 3.5-5$ dB/cm depending on the sample) [54]. Even more significant is the difference to femtosecond laser written waveguides. In this regard, Tan *et al.* have

Table 1.   Comparison of Various Integrated Optical Waveguides

Process Method	Source	Length-Dependent Attenuation in dB/cm	Dimensions	Shape
Doctor-blading copper cavities	[38]	1.1–4.4	60 µm × 60 µm	u-shaped
Flexographic printing	[51,54,55]	0.95–2.59	500 µm × 60 µm	circle segment
fs-writing in Glass	[3–5,7]	0.062–5.3	5–60 µm	round
Hot embossing	[56,57]	0.09–0.74	60 µm × 60 µm	square
Ion exchange	[10,11]	0.059–0.6	6–12 µm	elliptical
LDB		**0.258 ± 0.204**	**50 µm × 44 µm**	**u-shaped**
Mosquito	[58]	0.44	3.8–8.3 µm	round
OPTAVER	[36,59]	0.55 ± 0.243	300 µm × 45 µm	circle segment
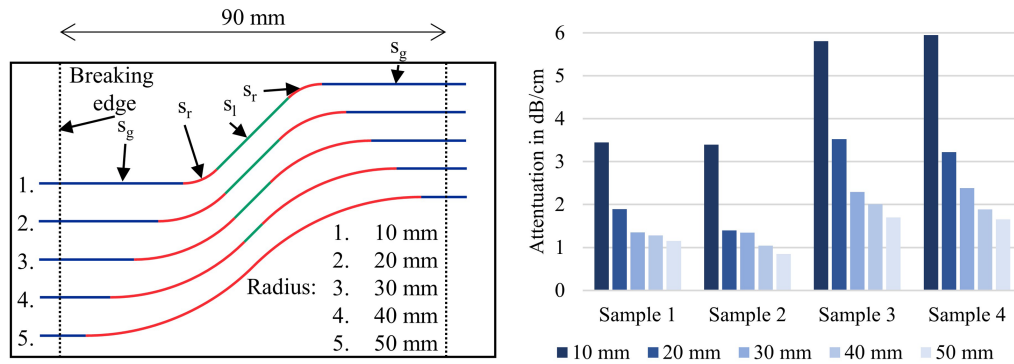
Fig. 9. Sample design to determine optical attenuation in terms of different radii of curvature (left), length-dependent attenuation of four different samples about the radius of curvature (right).

published that depending on the laser power during the writing process, the optical attenuation of the waveguides is $a_{15\,\mathrm{mm-tan}} = 6-55\,\mathrm{dB/cm}$ and at a larger radius up to $a_{30\,\mathrm{mm-tan}} = 22\,\mathrm{dB/cm}$ [62]. Tong *et al.* report similarly high losses of $a_{10\,\mathrm{mm-tong}} = 20\,\mathrm{dB/cm}$ and optical attenuation of $a_{20\,\mathrm{mm-tong}} = 8\,\mathrm{dB/cm}$ [63].

4. OUTLOOK AND SUMMARY

This paper presents a novel method for optical waveguide manufacturing called LDB. Here, continuous grooves are produced on thin glass surfaces using the LIDE method. Three strategies are discussed for filling these grooves with an optical polymer; the doctor-blade technique is demonstrated to be most suitable for this purpose. Regarding their geometrical properties and optical characteristics, multimodal optical waveguide structures are investigated and evaluated. A length-dependent optical attenuation of 0.258 dB/cm is achieved. Furthermore, the influence of the radii of curvature 10–50 mm along the waveguide is also analyzed. High optical losses occur at small radii and during coupling. In the future, based on this investigation, smaller and only single-mode capable structures can be fabricated with automated process chains. Especially moving the production site to a clean-room environment to fill the cavities and using automated end facet machining to be suitable for many more applications, as shown in the visionary approach of Fig. 1.

Disclosures. The authors declare no conflicts of interest.

Data availability. Data underlying the results presented in this paper are not publicly available at this time but may be obtained from the authors upon reasonable request.

REFERENCES

1. S. Miao, T. Liu, Y. Du, *et al.*, "2D material and perovskite heterostructure for optoelectronic applications," Nanomaterials **12**, 2100 (2022).
2. I. Konidakis, A. Karagiannaki, and E. Stratakis, "Advanced composite glasses with metallic, perovskite, and two-dimensional nanocrystals for optoelectronic and photonic applications," Nanoscale **14**, 2966–2989 (2022).
3. R. Ferrini, "Laser-based glass micromachining for integrated photonics," Photon. Views **20**, 56–60 (2023).
4. D. Tan, X. Sun, and J. Qiu, "Femtosecond laser writing low-loss waveguides in silica glass: highly symmetrical mode field and mechanism of refractive index change," Opt. Mater. Express **11**, 848–857 (2021).
5. M. Tunon de Lara, K. Chah, L. Amez-Droz, *et al.*, "Production of optical waveguide in planar glass substrate fabricated with femtoprint," Proc. SPIE **12142**, 121421K (2022).
6. G. Y. Chen, F. Piantedosi, D. Otten, *et al.*, "Femtosecond-laser-written microstructured waveguides in BK7 Glass," Sci. Rep. **8**, 10377 (2018).
7. J. Burghoff, S. Nolte, and A. Tünnermann, "Origins of waveguiding in femtosecond laser-structured LiNbO₃," Appl. Phys. A **89**, 127–132 (2007).
8. G. C. Righini and A. Chiappini, "Glass optical waveguides: a review of fabrication techniques," Opt. Eng. **53**, 071819 (2014).
9. S. Berneschi, G. C. Righini, and S. Pelli, "Towards a glass new world: the role of ion-exchange in modern technology," Appl. Sci. **11**, 4610 (2021).
10. H. Schröder, J. Schwietering, G. Böttger, *et al.*, "Hybrid photonic system integration using thin glass platform technology," J. Opt. Microsyst. **1**, 033501 (2021).
11. L. Brusberg, A. R. Zakharian, Ş. E. Kocabaş, *et al.*, "Glass substrate with integrated waveguides for surface mount photonic packaging," J. Lightwave Technol. **39**, 912–919 (2021).
12. J. Schwietering, C. Herbst, O. Kirsch, *et al.*, "Integrated optical single-mode waveguide structures in thin glass for flip-chip PIC assembly and fiber coupling," in *IEEE 70th Electronic Components and Technology Conference (ECTC)* (IEEE, 2020), pp. 148–155.
13. L. Brusberg, H. Schröder, C. Ranzinger, *et al.*, "Thin glass based electro-optical circuit board (EOCB) with through glass vias, gradient-index multimode optical waveguides and collimated beam mid-board coupling interfaces," in *IEEE 65th Electronic Components and Technology Conference (ECTC)* (IEEE, 2015), pp. 789–798.
14. A. Evertz, B. Reitz, E. Olsen, *et al.*, "Fast ethernet operation of a printed optical transmission path using industrial integration technologies," Proc. SPIE **12007**, 120070C (2022).
15. L. Brusberg, M. Neitz, D. Pernthaler, *et al.*, "Electro-optical circuit board with single-mode glass waveguide optical interconnects," Proc. SPIE **9753**, 97530J (2016).
16. T. Lamprecht, F. Betschon, J. Lambrecht, *et al.*, "EOCB-platform for integrated photonic chips direct-on-board assembly within Tb/s applications," in *IEEE 68th Electronic Components and Technology Conference (ECTC)* (IEEE, 2018), pp. 854–858.
17. A. Szameit, F. Dreisow, T. Pertsch, *et al.*, "Control of directional evanescent coupling in fs laser written waveguides," Opt. Express **15**, 1579–1587 (2007).

18. Y. Xiao, M. Hofmann, Z. Wang, *et al.*, "Design of all-polymer asymmetric Mach–Zehnder interferometer sensors," Appl. Opt. **55**, 3566–3573 (2016).

19. Y. Xiao, A. Langenecker, M. Hofmann, *et al.*, "Multimode interference structures as sensing elements integrated into Mach-Zehnder interferometers in polymer foils," Proc. SPIE **10025**, 100250V (2016).

20. R. Wolf, I. Breunig, H. Zappe, *et al.*, "Cascaded second-order optical nonlinearities in on-chip micro rings," Opt. Express **25**, 29927–29933 (2017).

21. E. Pichler, K. Bethmann, U. Zywietz, *et al.*, "Ring resonators in polymer foils for sensing of gaseous species," Proc. SPIE **9486**, 948613 (2015).

22. G. Ding, B. Ma, Y. Yan, *et al.*, "Through glass vias by wet-etching process in 49% HF Solution using an AZ4620 enhanced Cr/Au mask," in *IEEE 16th International Conference on Nano/Micro Engineered and Molecular Systems (NEMS)* (IEEE, 2021), pp. 872–875.

23. F. Ceyssens and R. Puers, "Deep etching of glass wafers using sputtered molybdenum masks," J. Micromech. Microeng. **19**, 67001 (2009).

24. N. Burshtein, S. T. Chan, K. Toda-Peters, *et al.*, "3D-printed glass microfluidics for fluid dynamics and rheology," Curr. Opin. Colloid Interface Sci. **43**, 1–14 (2019).

25. A. Butkutė, T. Baravykas, J. Stančikas, *et al.*, "Optimization of selective laser etching (SLE) for glass micromechanical structure fabrication," Opt. Express **29**, 23487–23499 (2021).

26. J. Gottmann, M. Hermans, and J. Ortmann, "Subtractive 3D printing glass by SLE: applications and combination with ultrafast laser glass welding (Conference Presentation)," Proc. SPIE **10908**, 109080D (2019).

27. R. Ostholt, "Method for microstructuring a glass substrate by means of laser radiation," U.S. patent 000011505495B2 (28 January 2020).

28. N. Ambrosius and R. Ostholt, "Method for producing microstructures in a glass substrate," U.S. patent 000011377387B1 (23 April 2020).

29. R. Santos, N. Anspach, N. Ambrosius, *et al.*, "Fabrication of panel-level glass substrates with complete design freedom using LIDE," in *IMAP Source Proc.* (2022), 000371.

30. "High aspect ratio glass microfluidics," Vitrion, 2023, https://www.vitrion.com/en/applications/microfluidics/.

31. R. Santos, N. Ambrosius, R. Ostholt, *et al.*, "Bringing new life to glass for wafer-level packaging applications," in *International Wafer Level Packaging Conference (IWLPC)* (IEEE, 2020), pp. 1–7.

32. R. Santos, J.-P. Delrue, N. Ambrosius, *et al.*, "Processing glass substrate for advanced packaging using laser induced deep etching," in *IEEE 70th Electronic Components and Technology Conference (ECTC)* (IEEE, 2020), pp. 1922–1927.

33. R. A. Krüger, M. Schulz-Ruhtenberg, B. Rösener, *et al.*, "LIDE: high aspect ratio glass processing technology for the mass production of microfluidic devices for biomedical applications," Proc. SPIE **10875**, 2509899 (2019).

34. B. Reitz, G. A. Hoffmann, S. N. Gottwald, *et al.*, "Fabrication of an integrated optical system in glass using laser assisted manufacturing," Proc. SPIE **11815**, 118150B (2021).

35. B. Hachicha and L. Overmeyer, "Functionalization of UV-curing adhesives for surface-integrated micro-polymer optical fibers," Proc. SPIE **9750**, 97500J (2016).

36. G.-A. Hoffmann, T. Reitberger, J. Franke, *et al.*, "Conditioning of surface energy and spray application of optical waveguides for integrated intelligent systems," Procedia Technol. **26**, 169–176 (2016).

37. M. D. Tyona, "A theoretical study on spin coating technique," Adv. Mater. Res. **2**, 195–208 (2013).

38. M. Siesicki, K. Nieweglowski, K. J. Wolter, *et al.*, "Integrated optical waveguides for electrooptical PCB," in *International Students and Young Scientists Workshop - Photonics and Microsystems* (IEEE, 2008), pp. 76–79.

39. B. Hachicha and L. Overmeyer, "In-line production, optronic assembly and packaging of POFs," Procedia Technol. **15**, 129–137 (2014).

40. T. Reitberger, G.-A. Hoffmann, T. Wolfer, *et al.*, "Printing polymer optical waveguides on conditioned transparent flexible foils by using the aerosol jet technology," Proc. SPIE **9945**, 99450G (2016).

41. M. A. Uddin, H. P. Chan, C. K. Chow, *et al.*, "Effect of spin coating on the curing rate of epoxy adhesive for the fabrication of a polymer optical waveguide," J. Elec. Mater. **33**, 224–228 (2004).

42. M.-A. Mattelin, J. Missinne, B. de Coensel, *et al.*, "Imprinted polymer-based guided mode resonance grating strain sensors," Sensors **20**, 3221 (2020).

43. J. Missinne, M.-A. Mattelin, N. T. Benéitez, *et al.*, "Comparison of different polymers and printing technologies for realizing flexible optical waveguide Bragg grating strain sensor foils," Proc. SPIE **10915**, 17 (2019).

44. M. Wang, J. Hiltunen, S. Uusitalo, *et al.*, "Fabrication of optical inverted-rib waveguides using UV-imprinting," Microelectron. Eng. **88**, 175–178 (2011).

45. D. Weyers, A. Mistry, K. Nieweglowski, *et al.*, "Hybrid lithography approach for single mode polymeric waveguides and out-of-plane coupling mirrors," in *IEEE 72nd Electronic Components and Technology Conference (ECTC)* (IEEE, 2022), pp. 1919–1926.

46. F. P. Bowden, F. P. Bowden, and D. Tabor, *The Friction and Lubrication of Solids* (Oxford University, 2001).

47. M. Siesicki, K. Nieweglowski, K.-J. Wolter, *et al.*, "Development of sol-gel integrated optical waveguide for electro-optical PCB," in *31st International Spring Seminar on Electronics Technology* (IEEE, 2008), pp. 222–227.

48. K. Nieweglowski and K.-J. Wolter, "Optical analysis of short-distance optical interconnect on the PCB-level," in *1st Electronic System Integration Technology Conference* (IEEE, 2006), pp. 392–397.

49. T. Bierhoff, A. Wallrabenstein, A. Himmler, *et al.*, "Ray tracing technique and its verification for the analysis of highly multimode optical waveguides with rough surfaces," IEEE Trans. Magn. **37**, 3307–3310 (2001).

50. M. Dumke, "Untersuchungen zur optischen Dämpfung mikrodispensierter Wellenleiter," Dissertation (Gottfried Wilhelm Leibniz Universität Hannover/TEWISS, 2015).

51. T. Wolfer, P. Bollgruen, D. Mager, *et al.*, "Printing and preparation of integrated optical waveguides for optronic sensor networks," Mechatronics **34**, 119–127 (2016).

52. Y. Koike, *Fundamentals of Plastic Optical Fibers* (Wiley, 2014).

53. A. Peczek, C. Mai, G. Winzer, *et al.*, "Comparison of cut-back method and optical backscatter reflectometry for wafer level waveguide characterization," in *IEEE 33rd International Conference on Microelectronic Test Structures (ICMTS)* (IEEE, 2020), pp. 1–3.

54. T. Wolfer, "Additive Fertigung integrierter multimodaler Polymer-Lichtwellenleiter mittels Flexodruck," Dissertation (TEWISS, 2020).

55. K. Pflieger, B. Reitz, G.-A. Hoffmann, *et al.*, "Layout optimization for flexographically printed optical networks," Appl. Opt. **60**, 9828–9836 (2021).

56. M. Rezem, Replication of Planar Polymer Micro-Optical Waveguides and Components (2019).

57. M. Rezem, A. Gunther, B. Roth, *et al.*, "Low-cost fabrication of all-polymer components for integrated photonics," J. Lightwave Technol. **35**, 299–308 (2017).

58. Y. Kobayashi, Y. Sakaguchi, K. Yasuhara, *et al.*, "Mosquito method based polymer tapered waveguide as a spot size converter," Opt. Express **29**, 9513–9531 (2021).

59. M.-K. Hamjah, J. Zeitler, Y. Eiche, *et al.*, "Manufacturing of polymer optical waveguides for 3D-opto-MID: review of the OPTAVER process," in *14th International Congress Molded Interconnect Devices (MID)* (IEEE, 2021), pp. 1–11.

60. N. D. Psaila, "3D laser direct writing for advanced photonic integration in optical communications," Proc. SPIE **10924**, 109240U (2019).

61. S. Serecunova, D. Seyringer, F. Uherek, *et al.*, "Waveguide shape and waveguide core size optimization of Y-branch optical splitters up to 128 splitting ratio," Opt. Commun. **501**, 127362 (2021).

62. D. Tan, X. Sun, Z. Li, *et al.*, "Effectively writing low propagation and bend loss waveguides in the silica glass by using a femtosecond laser," Opt. Lett. **47**, 4766–4769 (2022).

63. L. Tong, R. R. Gattass, I. Maxwell, *et al.*, "Optical loss measurements in femtosecond laser written waveguides in glass," Opt. Commun. **259**, 626–630 (2006).